Cation dopant distributions in nanostructures of transition-metal doped ZnO: Monte Carlo simulations

Timothy C. Droubay,[1] Tiffany C. Kaspar,[1] Bryce P. Kaspar,[2] and Scott A. Chambers[1]
[1]*Fundamental and Computational Sciences Directorate, Pacific Northwest National Laboratory, Richland, Washington 99352, USA*
[2]*Environmental Molecular Sciences Laboratory, Pacific Northwest National Laboratory, Richland, Washington 99352, USA*
(Received 17 October 2008; published 26 February 2009)

Monte Carlo simulations of cation doping within the ZnO lattice were utilized to evaluate dopant distributions in nanoparticles and thin films. In structures with a high surface-to-volume ratio, dopant distributions deviate significantly from predictions based on probabilistic expressions for infinitely large bulk lattices. We present empirical expressions that accurately predict dopant bonding configurations as a function of film or particle size, shape, and dopant concentration for any substitutional dopant (cation or anion) within a tetrahedrally coordinated compound, including zinc-blende, wurtzite, and diamond structures.

DOI: 10.1103/PhysRevB.79.075324 PACS number(s): 75.75.+a, 75.70.−i, 75.50.Pp

To synthesize materials with qualitatively new functionality in fields such as spintronics,[1] thermal and photocatalysis,[2] solar energy harvesting,[3] light emission,[4] and medical technology,[5] doping at relatively high concentrations (several at. %) is required. At these higher concentrations, the statistical probability governing the placement of each dopant in the host lattice will lead to a substantial quantity of dopant pairs (dimers), trimers, and so on; these clusters can have significant influence on the resultant material properties. For several common bulk lattices, Behringer[6] determined the statistical distribution of dopant singles, dimers, and trimers. However, for epitaxial films and nanoparticles, where much of the current interest resides, dopant distributions are substantially altered by the presence of undercoordinated surface sites.

Even when the dopant distribution remains stochastic, dopant proximities can vary widely as the dopant concentration increases, resulting in a range of interactions and associated properties. Accurately predicting dopant configurations within the host lattice enables such materials to be understood at a deeper level since dopant-dopant interactions can then be modeled based on realistic spatial distributions. Straightforward probabilistic approaches, such as the binomial theorem, work well for infinite bulk lattices where surface effects can be neglected. Assuming a completely random dopant distribution, Behringer[6] calculated statistical probabilities for singles, dimers, as well as open and closed trimers for several common lattice types. Attempts to empirically test the accuracy of the equations derived by Behringer used simple linear distances between dopants as the primary determinant of interaction.[7,8] It was shown that this approach can be problematic because in lattices involving hexagonally close-packed (HCP) stacking, the same distance between dopants is found for different bonding configurations.[9] Liu *et al.*[10] expanded Behringer's treatment and calculated the probabilities of six different kinds of tetramers for cations arranged in a face-centered-cubic lattice. However, nanocrystalline materials and thin films have a much larger surface-to-volume (S/V) ratio than bulk materials, and these calculations do not account for the reduced coordination at the surface of the host, which is a critical factor in determining the overall dopant distribution in low-dimensional systems in the nanometer or mesoscale range. As the nanoparticle size decreases, the ratio of surface to bulk lattice sites increases; thus, the error associated with assuming a bulklike probability distribution of the kind used by Behringer[6] increases as particle size drops. This effect was partially addressed by Suyver *et al.*,[7] who introduced a dimensionless variable to approximate the number of dimers in nanocrystalline particles of the zinc-blende structure. However, this method of calculating dimers breaks down for higher doping levels because trimers, tetramers, etc., which become very important at these higher doping levels, are not distinguished as such but are counted as combinations of dimers. As a result, the dimer fraction is severely overestimated at higher dopant fractions.

Here we evaluate the deviation from Behringer's statistical predictions for low-dimensional systems by performing Monte Carlo simulations of dopant distributions in which the nanoparticle size, shape, and dopant concentration are systematically varied. By empirically determining the probability of forming clusters with up to 20 dopant atoms per cluster, a clear dependence of dopant distribution on the size and shape of the host material emerges. Significantly, the dopant distribution approaches statistical predictions only in the limit of infinitely large lattices with nearly zero S/V ratio.

The importance of this phenomenon is illustrated using transition-metal doped wurtzite ZnO. To realize a dilute magnetic semiconductor for spintronics applications, transition-metal dopants with unpaired d electrons, such as Mn or Co, are expected to interact ferromagnetically in a nonmagnetic host such as ZnO.[1,11,12] However, pairs of dopants separated by intervening oxygen atoms usually align antiferromagnetically due to superexchange in both the wurtzite and zinc-blende structures.[12] The total magnetic moment expected for such a material then depends critically upon the average magnetic moment and population distribution for each cluster size and type.

Dopant clustering is described in terms of an "n-mer," which is defined as n dopant cations directly connected through intervening oxygen atoms. In the hexagonal wurtzite structure of ZnO, the cations are arranged in a HCP structure with 12 nearest-neighbor (NN) cation sites. An isolated dopant (M), or "single," has no additional dopants within the

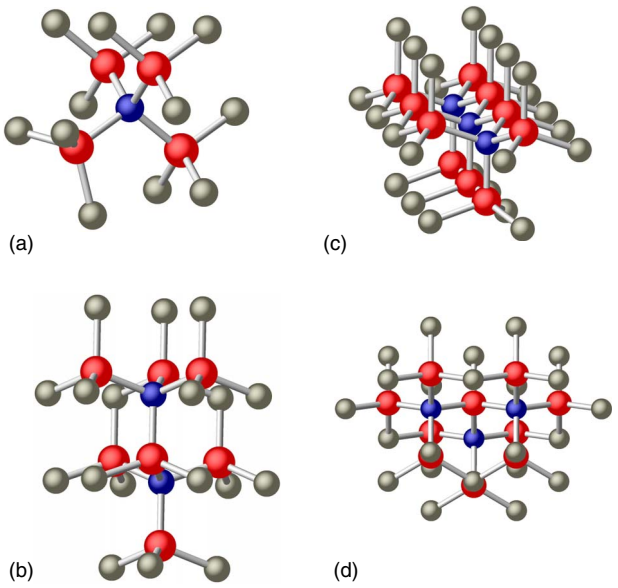

FIG. 1. (Color online) Typical representations of dopant configurations for (a) singles, (b) dimers, (c) and open and (d) closed trimers. Small dark blue: dopant; small light gray: Zn; large dark red: O.

first NN cation shell, as seen in Fig. 1(a). A dimer ($n=2$) is a cluster in which there is a second dopant in the NN cation shell surrounding the primary dopant. The second dopant does not have any additional NN dopants beyond the first dopant, as seen in Fig. 1(b). For higher-order clusters ($n>2$), distinctions can be made between different cluster geometries or types. For instance, two kinds of trimers ($n=3$), open and closed, are seen in Figs. 1(c) and 1(d). A good description of various cluster types in the zinc-blende structure and their respective magnetizations can be found in the review of the magnetization step method by Shapira and Bindilatti.[9]

A set of 1000 iterations was performed for each nanocrystalline geometry, size, and dopant concentration in order to statistically sample all possible outcomes. Typical results are summarized in the inset of Fig. 2 as histograms representing singles, dimers, and trimers for a 9% cation-doped ZnO ($M_{0.09}Zn_{0.91}O$) spherical nanoparticle of radius 5 nm. The probability distributions are well fit to Gaussians, indicating a normal distribution with a standard deviation of ~0.015 (fractional probability). We show in Fig. 2 the computed probabilities for singles, dimers, and trimers as a function of dopant concentration (x) between 0.001 and 0.20 for the same 5 nm radius spherical nanoparticle of $M_xZn_{1-x}O$. The solid lines are best fits to the data based on the binomial theorem functional form $P(x)=Cx^n(1-x)^k$, where C, n, and k were allowed to vary. Fitting the Monte Carlo simulations to this analytical function allows one to easily generate probabilities for the various configurations at any x value. As expected, isolated dopants dominate the distribution for concentrations less than $x=0.02$, and above this point higher-order clusters become appreciable.

To illustrate the deviation from bulk clustering probabilities for low-dimensional systems, Fig. 3 shows the influence of nanosphere size on dopant distribution for $M_{0.09}Zn_{0.91}O$.

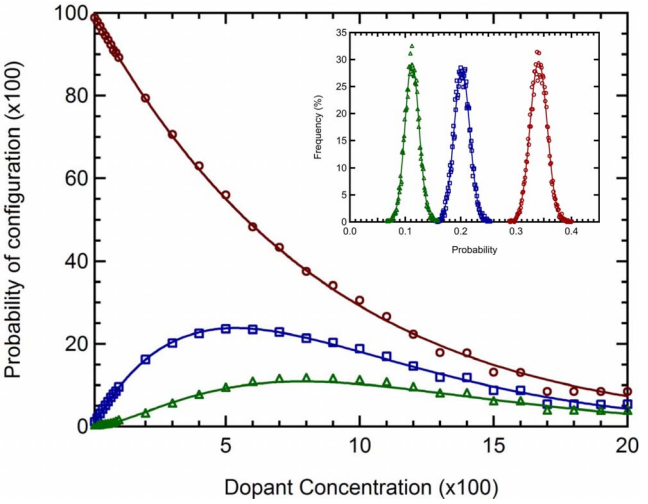

FIG. 2. (Color online) Monte Carlo probability for singles (red circles), dimers (blue squares), and trimers (green triangles) vs x for a random distribution of cation dopants within a 50 Å radius particle of $M_xZn_{1-x}O$. The solid lines are best fits assuming the functional form of binomial distribution but with different exponents determined by fitting. A particle of this size, shown in the inset, contains ~20 550 cation sites. Figure 3 Monte Carlo probability for singles (red circles), dimers (blue squares), and trimers (green triangles) vs x for a random distribution of cation dopants within a 50 Å radius particle of $M_xZn_{1-x}O$. The solid lines are best fits assuming the functional form of binomial distribution but with different exponents determined by fitting. Inset: probability distributions for singles (red circles), dimers (blue squares), and trimers (green triangles) for a 50 Å radius spherical nanoparticle of $M_{0.09}Zn_{0.91}O$.

Here we plot the Monte Carlo simulations for isolated dopant (a) singles and (b) dimers as a function of the S/V ratio for the particle. The S/V ratio is utilized as a convenient approximation to the ratio of surface cations with reduced coordination to bulk cations. The probabilities determined empirically are only identical to those calculated using Behringer's probabilistic formulas for S/V ratios approaching zero. For small nanoparticles (radii of a few nanometers), the Behringer equations predicts ~13% fewer singles and ~6% fewer dimers than the Monte Carlo simulation.

This result is of significant importance not only for spherical nanoparticles but also for nanostructures and thin films of other shapes with a S/V ratio of $\sim 5\times 10^{-4}$ Å^{-1} or higher (i.e., equivalent to that of a sphere of radius ~60 nm or less). These calculations were carried out using a variety of structures including spherical particles, thin disks, nanorods, and granular thin films. We introduce an "effective" concentration x_{eff} to account for the reduced coordination of the surface cations in the nanoparticles. The effective concentration x_{eff} is given by

$$x_{\text{eff}} = 1 - [(1-x)^{12} + 0.39S/V]^{1/12}. \quad (1)$$

Here, S and V are the surface area (in Å^2) and volume (in Å^3), respectively. For these diverse shapes, the probability of an isolated dopant (a single), dimers, and trimers can then be determined for actual concentrations between $x=\sim 0.05$ and

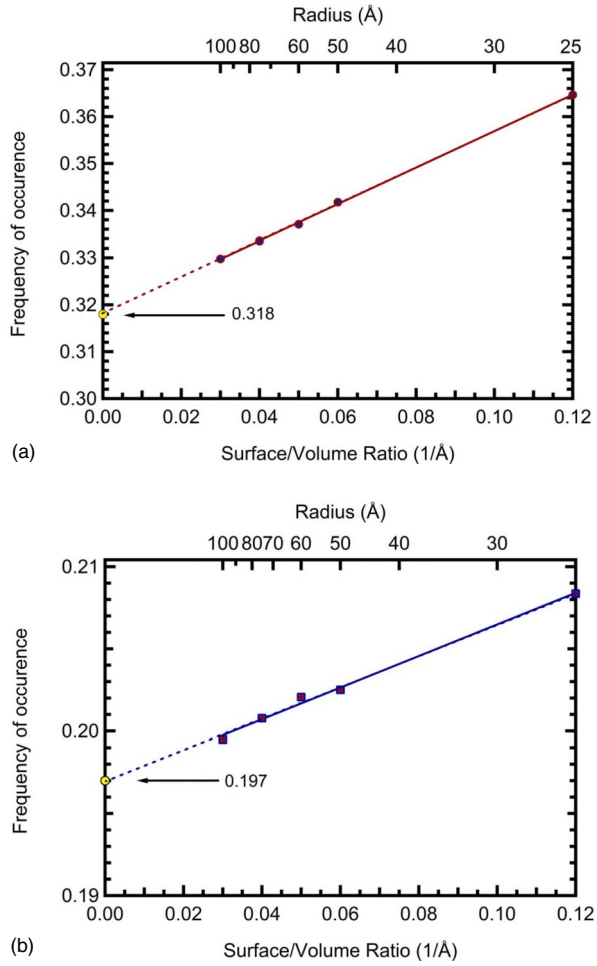

FIG. 3. (Color online) Probabilities of (a) single and (b) dimer formation for stochastic cation substitution in $M_{0.09}Zn_{0.91}O$ as a function of surface-to-volume ratio (S/V). The corresponding probabilistic values for an infinitely large crystal are shown at $S/V=0$.

$x=\sim 0.15$ by utilizing the probabilistic bulk formulas[6] with the effective cation concentration (x_{eff}) rather than the experimentally determined value (x). Since the reduced surface coordination of structures with large S/V values effectively lowers the concentration (increases the probability of singles), Eq. (1) is no longer valid at low x, as x_{eff} becomes negative.

As an example to illustrate the importance of these results, we consider magnetically doped ZnO. Thin films of transition-metal doped ZnO have been of enormous recent interest due to their intriguing but widely varying magnetic properties.[11–13] We have grown epitaxial films of Co:ZnO and Mn:ZnO on α-Al_2O_3(001) using pulsed laser deposition as described in detail elsewhere.[14,15] ZnO(001) grows in a columnar microstructure on α-Al_2O_3(001) due to the large (18%) lattice mismatch between the c plane of sapphire and that of ZnO. Hexagonal columns which average ~75 Å on a side and ~1000 Å tall are found by transmission electron microscopy throughout these films.[14] We have carried out Monte Carlo simulations to predict the dopant distribution in doped ZnO oxide pillars of this size ($S/V=5.4\times10^{-2}$ Å^{-1}). Figure 4 shows the results for $M_{0.10}Zn_{0.90}O$ using this columnar geometry for cluster sizes up to $n=20$. Clusters of tetramers or higher ($n\geq 4$) comprise a large fraction (40%) of the total number of dopants. As has been shown previously, these dopant clusters are expected to exhibit very different magnetic properties from those of isolated singles.[16] Figure 4 also shows the normalized total magnetic moment which would be expected assuming that antiferromagnetic superexchange dominates the interactions for nearest neighbors and that there is no anisotropy. In this generalized approach, an isolated dopant atom would have a normalized magnetic moment of 1, and dimers would align antiferromagnetically with a net moment of zero. This interaction results in zero average moment for all clusters of even n value and a total of one uncompensated spin per cluster for all clusters of odd n value. For simplicity, more complicated spin arrangements based upon cluster types, such as a spin-frustrated trimer, are neglected. In this scenario, 30.5% of the normalized moment would originate from isolated dopants (singles). In contrast, the bulk probabilistic model predicts 28.2%. In addition, the Monte Carlo simulations predict a maximum expected moment of 36.7% of the spin-only value, compared to only 32.4% calculated using singles and trimers of the bulk probabilistic model. For a dopant concentration of $x=0.10$ in ZnO, the predicted maximum magnetic moment for $Co_{0.10}Zn_{0.90}O$ is reduced from $4.8\mu_B$/Co to $1.76\mu_B$/Co atom while that for $Mn_{0.10}Zn_{0.90}O$ is $2.16\mu_B$/Mn rather than the spin-only moment of $5.9\mu_B$/Mn. These values can be compared with the bulk statistical predicted moments of 1.55 and 1.91 for $Co_{0.10}Zn_{0.90}O$ and $Mn_{0.10}Zn_{0.90}O$, respectively. Magnetization step studies in $Mn_xZn_{1-x}O$ confirm the dominant magnetic contribution from singles.[16]

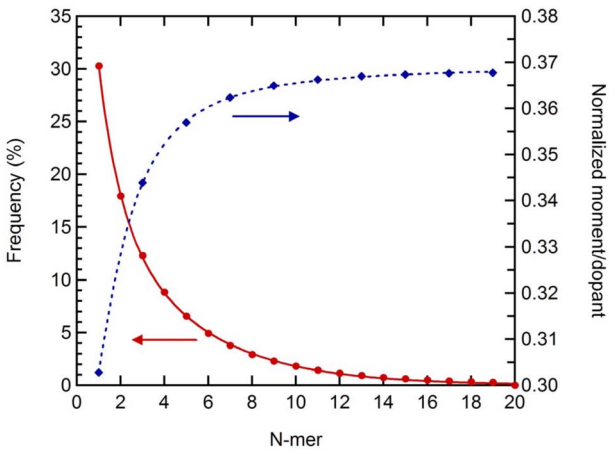

FIG. 4. (Color online) Frequencies of n-mer ($n=1-20$) configurations (closed red circles) for random cation substitution in $M_{0.10}Zn_{0.90}O$, assuming an oriented columnar geometry as is present in (001)-oriented epitaxial films grown on c-plane sapphire. Expected values for the normalized spin-only moment (blue diamonds) assuming superexchange for all even n-mers.

Varying the dopant concentration for this columnar microstructure generates a family of probability distribution curves, three of which are shown in Fig. 5(a). Numerical fits to these Monte Carlo data based on a log-normal distribution[17] [Eq. (2)] are shown in Fig. 5(b), where the data and fit for each concentration have been offset for clarity,

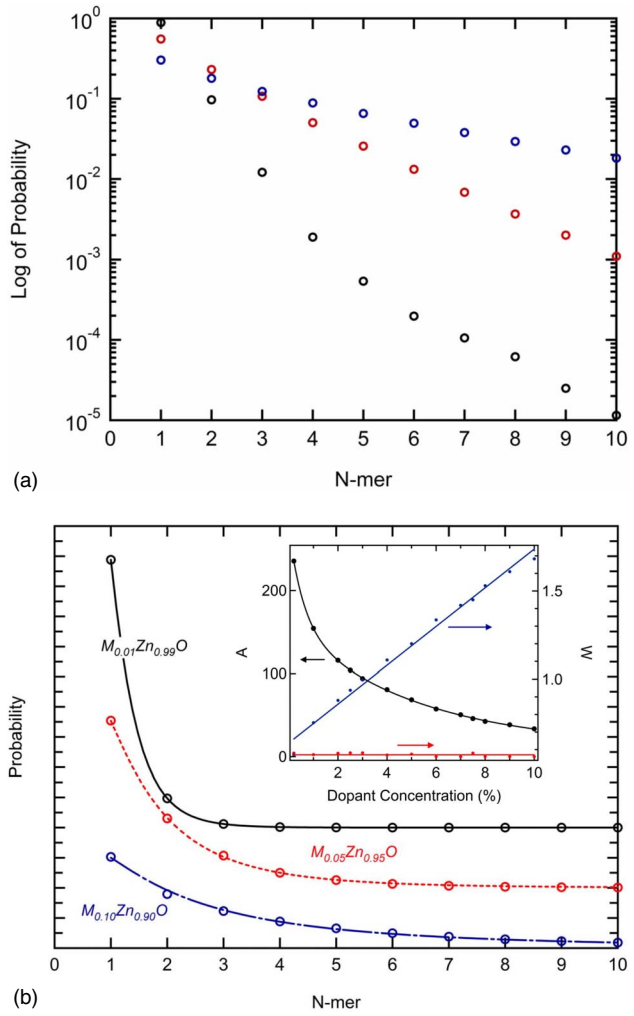

FIG. 5. (Color online) (a) Frequencies of n-mer ($n=1-10$) configurations (open circles) for random cation substitution in $M_{0.01}Zn_{0.99}O$ (black), $M_{0.05}Zn_{0.95}O$ (red), and $M_{0.10}Zn_{0.90}O$ (blue) in the same oriented columnar geometry as in Fig. 4. (b) Fits (solid curves) of the Monte Carlo simulations to a log-normal function [Eq. (2)] with coefficients that depend on the dopant concentration. These coefficients can in turn be fit using a power law, a line, and a constant (0.57) for the prefactor (A), width (w), and n_0, respectively, as seen in the inset.

$$P_n(x) = A(x)\exp\left\{-\left[\frac{\ln(n/n_0)}{w(x)}\right]^2\right\}. \quad (2)$$

The log-normal function uses coefficient values that are themselves functions of the concentration and have been determined by multiple simulations. The coefficients for the log-normal prediction are plotted in the inset of Fig. 5(b) as a function of dopant concentration. The prefactor (A) of the empirical prediction is best represented by a double exponential $A=12+110\exp(-x/0.006)+150\exp(-x/0.05)$. The width ($w$) increases linearly with cation concentration and is given by $w=11x+0.64$. The mean (n_0) decreases only slightly with increasing concentration and has only a marginal effect on the overall quality of the prediction; it is well represented by a constant $n_0=0.57$.

As shown above, the thin-film simulations for which dopants are assumed to be randomly distributed and homogeneous deviate from the bulk-based statistical prediction for singles, dimers, and trimers in systems with moderately high dopant concentrations ($x>0.05$). As might be anticipated, the deviation increases with increasing dopant concentration or decreasing nanoparticle grain size, reaching a maximum deviation of near 18% for $S/V\sim0.12$ Å^{-1} at $x=0.10$. This deviation agrees quite well with the empirical simulations by Suyver *et al.*[7] for dimers in nanoparticles with small dopant concentrations. However, in diluted magnetic semiconductors, dopant levels up to the cation percolation threshold (x_p) are of interest. Coey *et al.*[18] calculated the cation percolation thresholds for several candidate oxide-based semiconductor host lattices and obtained $x_p=0.18$ for ZnO. At this doping level, the method of Suyver *et al.*[7] for calculating dopant pairs is not accurate. In order to determine the finite-size effect for the columnar geometry described above at these higher concentrations, random and homogeneously doped ZnO thin-film simulations were carried out for $x=0.10-0.20$ and were tested against the approximation given in Eq. (2) and Fig. 5 generated from the Monte Carlo simulations for x between 0.001 and 0.10 (1000 iterations). This formula was then compared with Monte Carlo simulations for x between 0.10 and 0.20 carried out with fewer than 1000 iterations, typically 150–200, in order to conserve computer resources. Here the approximation agreed very well with simulations.

The present simulations and analysis were carried out for wurtzite ZnO. However, they can also be directly applied to any substitutionally doped tetrahedrally coordinated compound, including zinc-blende, wurtzite, and diamond structures, for either cation or anion dopants. While the overall prediction holds for the total number of n-mers for different lattice structures, the breakdown of cluster types within any n-mer will be different for each lattice. Moreover, there is a general implication from this work that transcends crystal structure—large errors will occur from the use of the bulk-derived statistical predictions of n-mer cluster distributions in nanostructures, thin films, and superlattices. Reduced coordination at the surface produces an effective concentration which is lower than the actual concentration, resulting in an enhancement of the proportion of lower n-mer clusters. Being cognizant of these reduced-dimensionality effects could prove critical in designing and controlling advanced materials for magnetic, optical, electronic, catalytic, and other functional materials in both nanoparticle and thin-film form. Indeed, such grand challenges as control of quantum coherence at the level of individual electrons in doped systems will require the ability to describe dopant distributions with a level of precision beyond that of bulk probabilistic methods. The physical understanding and associated formulas described here represent a step in this direction.

This work was supported by the Office of Science, Division of Materials Sciences and Engineering, U.S. Department of Energy. This work was performed in the Environmental Molecular Sciences Laboratory, a national scientific user facility sponsored by the Office of Biological and Environmental Research of the Department of Energy and located at Pacific Northwest National Laboratory.

[1] T. Dietl, J. Appl. Phys. **103**, 07D111 (2008).
[2] P. S. Casey, C. J. Rossouw, S. Boskovic, K. A. Lawrence, and T. W. Turney, Superlattices Microstruct. **39**, 97 (2006).
[3] D. J. Norris, A. L. Efros, and S. C. Erwin, Science **319**, 1776 (2008).
[4] Q. Y. Meng *et al.*, J. Appl. Phys. **102**, 093505 (2007).
[5] K. M. Krishnan, A. B. Pakhomov, Y. Bao, P. Blomqvist, Y. Chun, M. Gonzales, K. Griffin, X. Ji, and B. K. Roberts, J. Mater. Sci. **41**, 793 (2006).
[6] R. E. Behringer, J. Chem. Phys. **29**, 537 (1958).
[7] J. F. Suyver, R. Meester, J. J. Kelly, and A. Meijerink, J. Lumin. **102-103**, 182 (2003).
[8] H. Bednarski, J. Cisowski, and J. C. Portal, Phys. Rev. B **55**, 15762 (1997).
[9] Y. Shapira and V. Bindilatti, J. Appl. Phys. **92**, 4155 (2002).
[10] M. T. Liu, Y. Shapira, E. t. Haar, V. Bindilatti, and E. J. McNiff, Jr., Phys. Rev. B **54**, 6457 (1996).
[11] C. Liu, F. Yun, and H. Morkoc, J. Mater. Sci.: Mater. Electron. **16**, 555 (2005).
[12] J. K. Furdyna, J. Appl. Phys. **64**, R29 (1988).
[13] T. Dietl, J. Phys.: Condens. Matter **19**, 165204 (2007).
[14] T. Droubay, D. J. Keavney, T. C. Kaspar, S. M. Heald, C. A. Johnson, K. M. Whitaker, D. R. Gamelin, and S. A. Chambers (unpublished).
[15] T. C. Kaspar, T. Droubay, S. M. Heald, P. Nachimuthu, C. M. Wang, V. Shutthanandan, C. A. Johnson, D. R. Gamelin, and S. A. Chambers, New J. Phys. **10**, 055010 (2008).
[16] X. Gratens, V. Bindilatti, N. F. Oliveira, Y. Shapira, S. Foner, Z. Golacki, and T. E. Haas, Phys. Rev. B **69**, 125209 (2004).
[17] E. Limpert, W. A. Stahel, and M. Abbt, BioScience **51**, 341 (2001).
[18] J. M. D. Coey, M. Venkatesan, and C. B. Fitzgerald, Nature Mater. **4**, 173 (2005).